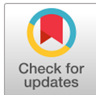

Research Article | Vol. 25, No. 25 | 11 Dec 2017 | OPTICS EXPRESS 32206
Optics EXPRESS

Transparent electrode design for AlGaN deep-ultraviolet light-emitting diodes

RAY- HUA HRONG,[1,2,*] YU-YUAN ZENG,[2] WEI-KAI WANG,[3] CHIA-LUNG TSAI,[4] YI-KENG FU,[4] AND WEI-HUNG KUO[4]

[1]*Institute of Electronics, National Chiao Tung University, Hsinchu 30010, Taiwan*
[2]*Graduate Institute of Precision Engineering, National Chung Hsing University 40227, Taiwan*
[3]*Department of Materials Science and Engineering, Da-Yeh University, Changhua 51591, Taiwan*
[4]*Electronic and Optoelectronic System Research Laboratories, ITRI, Hsinchu 31040, Taiwan*
[*]*rhh@nctu.edu.tw*

Abstract: Zinc gallate ($ZnGa_2O_4$; ZGO) thin films were employed as the p-type transparent contact layer in deep-ultraviolet AlGaN-based light-emitting diodes (LEDs) to increase light output power. The transmittance of 200-nm-thick ZGO in deep-ultraviolet wavelength (280 nm) was as high as 92.3%. Two different ohmic contact structures, a dot-LED (D-LED; ZGO/dot-ITO/LED) and whole-LED (W-LED; ZGO/ITO/LED), exhibited improved light output power and current spreading compared to a conventional ITO-LED (C-LED). At an injection current of 20 mA, the D-LED and W-LED exhibited 33.7% and 12.3% enhancements in light output power, respectively, compared to the C-LED. The enhanced light output power of the D-LED can be attributed to an improvement in current spreading and enhanced light-extracting efficiency achieved by introducing ZGO/dot-ITO.

© 2017 Optical Society of America under the terms of the OSA Open Access Publishing Agreement

OCIS codes: (230.3670) Light-emitting diodes; (250.0250) Optoelectronics.

References and links

1. H. Hirayama, N. Maeda, S. Fujikawa, S. Toyoda, and N. Kamata, "Recent progress and future prospects of AlGaN-based high-efficiency deep-ultraviolet light-emitting diodes," Jpn. J. Appl. Phys. **53**(10), 100209 (2014).
2. P. Dong, J. Yan, J. Wang, Y. Zhang, C. Geng, T. Wei, P. Cong, Y. Zhang, J. Zeng, Y. Tian, L. Sun, Q. Yan, J. Li, S. Fan, and Z. Qin, "282-nm AlGaN-based deep ultraviolet light-emitting diodes with improved performance on nano-patterned sapphire substrates," Appl. Phys. Lett. **102**(24), 241113 (2013).
3. M. Shatalov, W. Sun, A. Lunev, X. Hu, A. Dobrinsky, Y. Bilenko, J. Yang, M. Shur, R. Gaska, C. Moe, G. Garrett, and M. Wraback, "AlGaN deep-ultraviolet light-emitting diodes with external quantum efficiency above 10%," Appl. Phys. Express **5**(8), 082101 (2012).
4. Y. J. Jo, C. H. Hong, and J. S. Kwak, "Improved electrical and optical properties of ITO thin films by using electron beam irradiation and their application to UV-LED as highly transparent p-type electrodes," Curr. Appl. Phys. **11**(4), S143–S146 (2011).
5. S. L. Ou, D. S. Wuu, S. P. Liu, Y. C. Fu, S. C. Huang, and R. H. Horng, "Pulsed laser deposition of ITO/AZO transparent contact layers for GaN LED applications," Opt. Express **19**(17), 16244–16251 (2011).
6. T. Hoon Seo, B. Kyoung Kim, G. U. Shin, C. Lee, M. Jong Kim, H. Kim, and E.-K. Suh, "Graphene-silver nanowire hybrid structure as a transparent and current spreading electrode in ultraviolet light emitting diodes," Appl. Phys. Lett. **103**(5), 051105 (2013).
7. H. Ohta, K. Nomura, H. Hiramatsu, K. Ueda, T. Kamiya, M. Hirano, and H. Hosono, "Frontier of transparent oxide semiconductors," Solid-State Electron. **47**(12), 2261–2267 (2003).
8. H. J. Lee, J. W. Kang, S. H. Hong, S. H. Song, and S. J. Park, "$Mg_xZn_{1-x}O/Ag/Mg_xZn_{1-x}O$ M\multilayers as high-performance transparent conductive electrodes," ACS Appl. Mater. Interfaces **8**(3), 1565–1570 (2016).
9. V. Wang, W. Xiao, L. J. Kang, R. J. Liu, H. Mizuseki, and Y. Kawazoe, "Sources of n-type conductivity in $GaInO_3$," J. Phys. D **48**(1), 015101 (2014).
10. M. Orita, H. Ohta, M. Hirano, and H. Hosono, "Deep-ultraviolet transparent conductive β-Ga_2O_3 thin films," Appl. Phys. Lett. **77**(25), 4166–4168 (2000).
11. S. H. Yang, "Electrophoretic prepared $ZnGa_2O_4$ phosphor film for FED," J. Electrochem. Soc. **150**(10), H250–H253 (2003).
12. S. H. Wu and H. C. Chang, "Preparation and characterization of nanosized $ZnGa_2O_4$ phosphors," J. Electrochem. Soc. **151**(7), H159–H163 (2004).
13. S. Y. Bae, J. Lee, H. Jung, J. Park, and J. P. Ahn, "Helical structure of single-crystalline $ZnGa_2O_4$ nanowires," J. Am. Chem. Soc. **127**(31), 10802–10803 (2005).

#313104 https://doi.org/10.1364/OE.25.032206
Journal © 2017 Received 8 Nov 2017; revised 5 Dec 2017; accepted 6 Dec 2017; published 8 Dec 2017

14. L. Chen, D. Jiang, X. Liu, and G. Qiu, "$ZnGa_2O_4$ Nanorod Arrays Decorated with Ag Nanoparticles as Surface-Enhanced Raman-Scattering Substrates for Melamine Detection," ChemPhysChem **15**(8), 1624–1631 (2014).
15. S. J. Kim, H. H. Yoon, S. Y. Park, Y. S. Park, and H. W. Choi, "Synthesis of nanocrystalline $ZnGa_2O_4$ phosphor with different concentrations via a precipitation method," Jpn. J. Appl. Phys. **47**(1 1S), 784–786 (2008).
16. Y. S. Shen, W. K. Wang, and R. H. Horng, "Characterizations of metal-oxide-semiconductor field-effect transistors of ZnGaO grown on sapphire substrate," IEEE. J. Electron. Devices Soc. **5**(2), 112–116 (2017).
17. R. H. Horng, C. Y. Huang, S. L. Ou, T. K. Juang, and P. L. Liu, "Epitaxial growth of $ZnGa_2O_4$: A new deep ultraviolet semiconductor candidate," Cryst. Growth Des. (to be published).
18. H. Z. Xi, B. Y. Man, C. S. Chen, M. Liu, J. Wei, and S. Y. Yang, "Effects of annealing temperature on amorphous GaN films formed on Si(111) by pulsed laser deposition," Semicond. Sci. Technol. **24**(8), 085024 (2009).
19. W. K. Wang, S. Y. Huang, M. C. Jiang, and D. S. Wuu, "Optoelectronic properties and structural characterization of GaN thick films on different substrates through pulsed laser deposition," Appl. Sci. **7**(1), 87 (2017).
20. N. Nepal, M. L. Nakarmi, J. Y. Lin, and H. X. Jiang, "Photoluminescence studies of impurity transitions in AlGaN alloys," Appl. Phys. Lett. **89**(9), 092107 (2006).

1. Introduction

AlGaN-based deep-ultraviolet (DUV) light-emitting diodes (LEDs) with 280-nm wavelengths attract considerable attention for use in chemical sensors, biological detection, water purification, UV curing, and so on [1,2]. However, the external quantum efficiency (EQE) of UV LEDs is unsatisfactorily, partially because most of the emitted photons generated by the active region are absorbed by p-type contact layers, resulting in low light-extraction efficiency (LEE) [3]. Indium tin oxide (ITO) is generally inserted as a transparent conducting electrode (TCE) layer between p-GaN and the p-electrode to improve p-type ohmic contact, resulting in the formation of a current-spreading layer [4,5]. The ITO film has both high electrical conductivity along with excellent optical transmittance at near-UV to visible wavelengths. However, ITO film is opaque in DUV applications because of its small optical bandgap (~3.2 eV), which significantly reduces the transmittance in the UV region. Therefore, it is important to develop new transparent conductive oxide (TCO) materials with wide optical bandgaps as replacements for ITO thin films to improve the performance of UV LEDs [6]. The electron-release efficiencies of wide-bandgap TCOs are known to be lower than those of narrow-bandgap TCOs [7], limiting the candidate TCOs that can be applied at DUV wavelengths. The resistivities of wide-bandgap TCO materials such as $Mg_xZn_{1-x}O$, $In_xGa_{1-x}O$, and Ga_2O_3 are too high (on the order of 10^{-1}~10^{-3}) for application as TCEs in DUV LEDs [8–10].

Recently, zinc gallate ($ZnGa_2O_4$; ZGO) films (composites of Ga_2O_3 and ZnO) have been proposed as TCO materials for use in the DUV region because of their high chemical stability and large optical bandgap of 5.12 eV. $ZnGa_2O_4$ has a spinel crystal structure (cubic structure with space group $Fd_{3\,m}$) with the lattice parameters $a = b = c = 0.8335$ nm and $\alpha = \beta = \gamma = 90$, where Ga^{3+} ions occupy the octahedral sites, and Zn^{2+} ions occupy the tetrahedral sites. $ZnGa_2O_4$ has been reported to be favorable for application in field-emission displays with low accelerating voltages [11]. Most discussions on $ZnGa_2O_4$ focus on the one-dimensional nanostructure and optical emission properties of, for example, $ZnGa_2O_4$ nanoparticles, nanowires, and nanorods [12–15]. In our previous study, we discussed the device characteristics and optical properties of electronic devices containing ZGO epilayers [16]. In this study, we fabricated and optimized the crystalline quality of a ZGO thin film and evaluated the ZGO epilayer as a TCO for DUV LED applications. The electrical and optical properties of DUV LEDs containing ZGO-based ohmic-contact ITO TCE (ZGO:ITO) layers were also investigated.

2. Experimental

ZGO thin films were grown on *c*-plane (0001) sapphire substrates using a MOCVD system. Triethylgallium (TMGa), diethylzinc (DEZn), and oxygen gas were used as the precursors of Ga, Zn, and O, respectively, and Ar was used as the carrier gas. ZGO thin films were grown

at a temperature 670°C with different thicknesses of 25, 50, 75, 100, and 125 nm. The flow rate of TMGa was kept constant. The flow rates of the Zn source were 10, 20, 30, 40, 50, and 60 sccm, corresponding to a maximum Ga/Zn molar flow rate of 1:1.2. During the MOCVD process, oxygen flow was kept at 200 sccm, the growth pressure was 15 Torr, and the growth temperature was 670°C. The UV LEDs were grown on *c*-plane sapphire substrates with a 2-µm-thick undoped AlGaN template, a 2.5-µm-thick Si-doped n-AlGaN layer, multiple quantum wells consisting of nine pairs of AlGaNInN/AlGaN layers, a 40-nm-thick electron blocking layer, a 100-nm-thick Mg-doped p-AlGaN layer, and a 3-nm-thick p-GaN contact layer. ITO was deposited on the LEDs via e-beam evaporation at room temperature (RT) followed by annealing in nitrogen at 600°C for 20 min. The ITO target was a mixture of 10% SnO_2 and 90% In_2O_3 by weight. Ti/Al/Ti/Au metals (15/2000/60/20 nm) were used as metal pads in the UV LEDs. The UV LED chip size was 1 mm × 1 mm. ZGO was deposited as a TCE layer via MOCVD with a DEZn flow rate of 60 sccm, and the ZGO film thickness was increased to 100 nm to improve current spreading. Two TCE patterns, a dot-LED (D-LED; ZGO/dot-ITO/LED) and whole-LED (W-LED; ZGO/ITO/LED), were defined and etched using standard photo-lithography and inductively coupled plasma reactive-ion etching. The dot diameter and pitch were 100 and 175 µm, respectively. Figures 1(a)–1(m) show the fabrication processes for the conventional UV LED (C-LED), D-LED, W-LED and dot-ITO pattern design. Optical transmittance was measured in the range of 200 to 800 nm using an N&K analysis system. Structural properties were characterized by double-crystal X-ray diffraction (XRD), scanning electron microscopy, and atomic force microscopy. The electrical properties of the ZGO films were determined by Van der Pauw-Hall measurements at RT. The current–voltage (*I*–*V*) and output power characteristics of the three LEDs were measured at RT using a Keithley 2400 instrument with an integrating sphere detector.

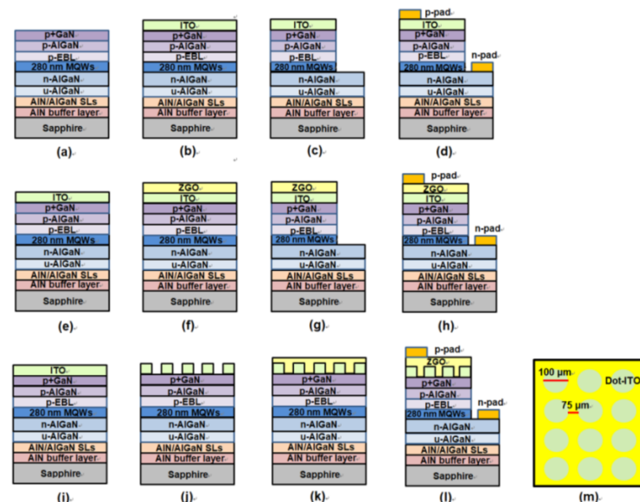

Fig. 1. Formation process of a C-LED: (a) epitaxial layer, (b) ITO deposition, (c) mesa, and (d) metal pad. Formation process of a W-LED: (e) ITO deposition on the epitaxial layer, (f) ZGO deposition, (g) mesa, and (h) metal pad. Formation process of a D-LED: (i) dot-ITO deposition, (j) ZGO deposition, (k) mesa, (l) metal pad, and (m) schematic diagram of ZGO/dot-ITO pattern design.

3. Results and Discussion

The effect of DEZn flow rate on the crystallinity of the ZGO films grown on sapphire substrates was investigated [17]. The DEZn flow rate varied from 10 to 60 sccm, while the O_2 flow rate was fixed at 200 sccm. Figure 2 shows the typical XRD patterns of ZGO films grown with different DEZn flow rates. The preferred ZnGaO crystal planes [(111), (222), and (333), as indicated by intense diffraction peaks at 18.57°, 37.61°, and 57.82°, respectively]

were observed, in agreement with the reported data (JCPDS card file 381240). It is worth noting that the diffraction peak at 57.82° was attributed to the (333) plane rather than the (511) plane because the ZGO film did not have a perfect structure. Compared with the XRD pattern of monoclinic β-Ga_2O_3 [diffraction at 18.95° corresponding to (–201) plane reflections], the diffraction peaks of the ZGO film shifted toward lower angles from 18.85° to 18.53° as the DEZn flow rate increased. This was attributed to the transferred most of Zn reacted with Ga and O atoms into the ZGO epilayer. To evaluate the quality of the ZnGaO film, the full width at half maximum (FWHM) of the (111) peak of the ZGO film was used to evaluate the crystallinity. The FWHM values for samples with DEZn flow rates of 10, 30, 40, 50, and 60 sccm were 0.592, 0.551, 0.474, 0.398, and 0.354, respectively. The FWHM decreased with increasing DEZn flow rate, reaching the minimum value of 0.354 at a flow rate of 60 sccm. The decrease in FWHM was attributed to the increase in crystallite size resulting from either the aggregation of small grains or grain boundary movement during the growth process [18]. The grain size of ZGO grown with different DEZn flow rates can be calculated using the Debye–Scherer equation [19]:

$$D = 0.9\lambda / \text{FWHM}\cos(\theta),$$

where D is the crystallite size, λ is the X-ray wavelength, and θ is the diffraction angle. The crystallite sizes of samples with DEZn flow rates of 10, 30, 40, 50, and 60 sccm were estimated to be 14.69, 14.61, 16.98, 20.23, and 23.33 nm, respectively. These results indicated that increasing in Zn content improved the crystallinity of the ZGO film, which can be explained as follows. With increasing Zn content, more ions Zn occupied the interstitial sites of Ga_2O_3 to substitution Ga sites, and the crystal structure changed from monolithic to a spinel structure.

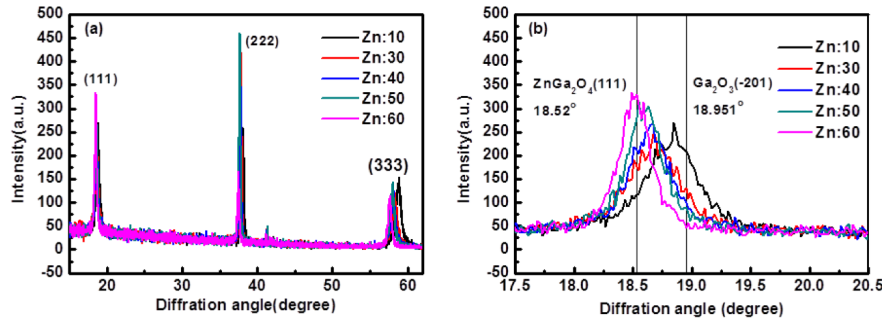

Fig. 2. (a) XRD data of ZGO films deposited under different DEZn flow rates and (b) magnification of the ZGO (111) diffraction peak.

The XRD data of the ZGO films are summarized in Table 1. Electrical resistivity is known to be inversely proportional to the carrier concentration and carrier mobility. The electrical resistivities of the films grown at different DEZn flow rates were determined from Hall measurements performed at RT [17]. The carrier concentration of the ZGO film deposited at a DEZn flow rate of 60 sccm was higher than those of the other films, whereas its carrier mobility was the lowest among all samples. It could be due to the fact that the existence of a high intrinsic defect and largest grain size for the ZGO thin film. The carrier concentration, mobility, and resistivity of the ZGO epilayer formed with a DEZn flow rate at 60 sccm were approximately 6.7×10^{16} cm^{-3}, 1.37 cm^2/V·s, and 67.9 Ω·cm, respectively. The ZGO epilayer grown at 60 sccm showed the best electrical properties. Thus, ZGO epilayers were grown at 60 sccm on the top layer of DUV LED epilayers (Z-LEDs) followed by thermal annealing at different temperatures. However, the results showed that the ZGO layer did not form an ohmic contact with the p + GaN contact layer, and the *I*–*V* characteristics of the Z-LED did not indicate normal diode performance. To overcome the barrier between

ZGO and the p + GaN top layer, an ITO layer was inserted between ZGO and p + GaN. Because the ZGO was grown at 670°C after ITO deposition, it was important to evaluate the electrical properties of ZGO grown on ITO with different thicknesses.

Table 1. Crystallinity Data of ZGO Thin Films.

DEZn flow rate	10 sccm	30 sccm	40 sccm	50 sccm	60 sccm
d-spacing (A)	2.356	2.37	2.37	2.38	2.39
FWHM (111)	0.592	0.551	0.474	0.398	0.354
grain size (nm)	14.69	14.61	16.98	20.23	23.32

Figure 3 shows the resistivity of ZGO (thickness = 200 nm)/ITO with different thicknesses. Because the electrical properties of ITO are better than those of 200-nm-thick ZGO, the resistivity of the ZGO/ITO bilayer improved as the ITO thickness increased. It is worth mentioning that the resistivity of ZGO (200 nm) deposited on ITO (25 nm) was approximately 4.82×10^{-3} Ω·cm, which is lower than that of the ZGO epilayer alone (67.9 Ω·cm). This means that the ITO layer can withstand the 670°C temperature during ZGO growth. Moreover, the resistivity of the bilayer decreased to 6.25×10^{-4} Ω·cm and became saturated as the ITO thickness increased to 125 nm. Because ITO is opaque at the wavelength of 280 nm, the thickness of ITO in the bilayer was 100 nm for the DUV LED evaluation.

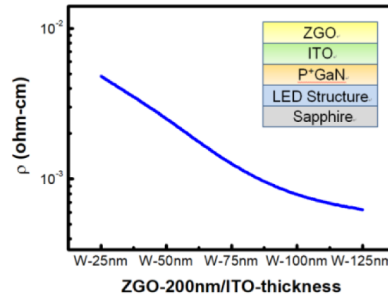

Fig. 3. Resistivity of ZGO (thickness = 200 nm) deposited on ITO with different thicknesses.

Figure 4 shows the optical transmittance data measured for ZGO deposited on ITO with different thicknesses and patterns. ITO with the dot form was also prepared for the transparency study. Figure 4(a) shows the measured optical transmittance spectra for the ZGO/ITO TCEs with different ITO layer thicknesses (ZGO film thickness was 200 nm) deposited on double-polished sapphire substrates. At a wavelength of 280 nm, the ZGO/ITO-25 nm, ZGO/ITO-50 nm, ZGO/ITO-100 nm, and ZGO/ITO-125 nm TCEs showed transmittance values of 60.7%, 33.5%, 32.8%, and 31.1%, respectively. The transmittance decreased with increasing ITO layer thickness because ITO exhibits strong absorption in the UV region. Considering the electrical and optical properties, the ZGO/ITO-100 nm thin film was chosen as the TCL for the LED in this study. Figure 4(b) shows the transmittances of ITO (200 nm), ZGO (200 nm), ZGO/ITO (200/100 nm) and ZGO/dot-ITO (200/100 nm). The dot diameter and pitch were 100 and 175 µm, respectively. ITO, ZGO, ZGO/ITO, and ZGO/dot-ITO showed transmittances of 28.3%, 93.2%, 32.8%, and 65.7%, respectively, at the wavelength of 280 nm. ZGO/dot-ITO exhibited much higher transmittance than the ITO film in the UV region because some of the UV light penetrated through the region without ITO. Thus, it was important to evaluate the performances of the DUV LEDs with different contact layers.

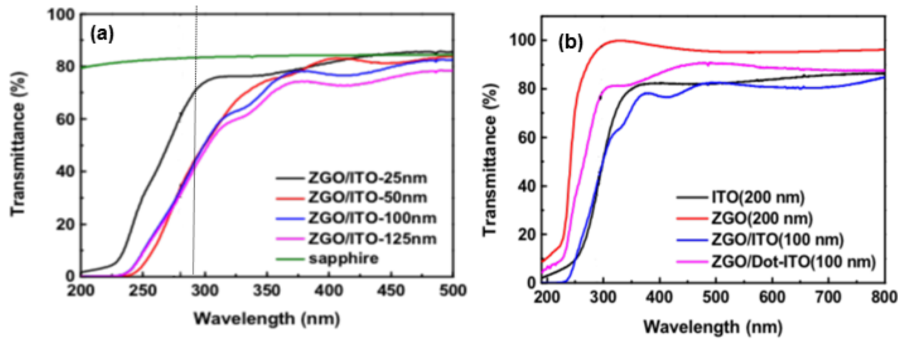

Fig. 4. (a) Optical transmittance data for ZGO/ITO samples with different film thicknesses (a) and structures (b).

Figure 5 shows the typical *I–V* characteristics of the UV LEDs fabricated using various TCEs. At an injection current of 20 mA, the C-LED, W-LED, and D-LED gave forward voltages of 7.6, 7.8, and 8.2 V, respectively. The ohmic contact area in ITO dot/p-GaN was reduced, causing the forward voltage of the D-LED to be slightly higher than those of the C-LED and W-LED. Furthermore, the Z-LED exhibited non-ohmic contact behavior. The forward voltage of an LED is correlated with the contact resistance of the TCE. It can be attributed to the high electrical resistance of the ZGO/p-GaN interface. The inset images in Fig. 5 show the three LED light patterns at the injection current of 20 mA. For the C-LED and W-LED, the photoemission was localized around the p-pad because of the current-crowding effect. The D-LED exhibited more uniform emission across the chip area compared to the C-LED and W-LED. This can be explained by the improvement in LEE attributed to the D-LED structure.

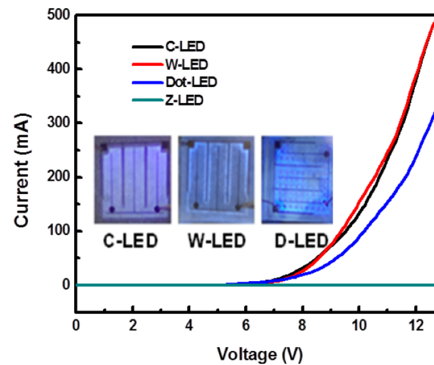

Fig. 5. Forward *I–V* characteristics of ZGO/ITO UV LEDs with different structures.

Figure 6(a) shows the output powers of the UV LEDs with lens encapsulation as a function of the injection current. At an injection current of 200 mA, the output powers of the C-LED, W-LED, and D-LED were 8.9, 10, and 11.8 mW, respectively. The output powers of the W-LED and D-LED were 12.4% and 32.6% higher than that of the C-LED, respectively. The higher output power is attributed to the improved current-spreading path in the W-LED and the higher LEE through ITO to ZGO in the D-LED. Figure 6(b) shows the electroluminescence (EL) spectra of the three UV LEDs at an injection current of 200 mA and RT. Single and sharp EL peaks at 280 nm were clearly observed for the devices, indicating that the highly crystalline ZGO film improved the optical performance of the DUV LEDs. Here, the broad emission band centered around 430 nm was also obtained. The origin of the violet-blue band is resulted from the group-III vacancy in the n-type AlGaN layer which plays the non-radiative recombination centers [20]. Figure 7(a) shows the wall-plug

Optics EXPRESS

efficiencies of the three LEDs as a function of current. The wall-plug efficiencies of the C-LED, W-LED, and D-LED at 20 mA were 2.8%, 2.45%, and 3.2%, respectively. At an injection current of 200 mA, the wall-plug efficiencies of the C-LED, W-LED, and D-LED were 0.41%, 0.49%, and 0.52, respectively. The wall-plug efficiency of the D-LED was better than those of the C-LED and W-LED. The EQE values of the LEDs are shown in Fig. 7(b) as a function of current. The EQE of the D-LED was clearly superior to those of the other LEDs.

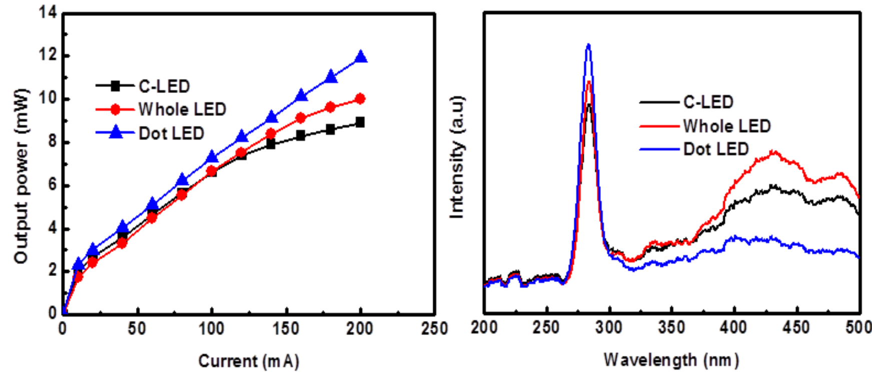

Fig. 6. (a) Light output power as a function of injection current and (b) EL emission spectra at 200 mA for the three types of ZGO/ITO UV LEDs.

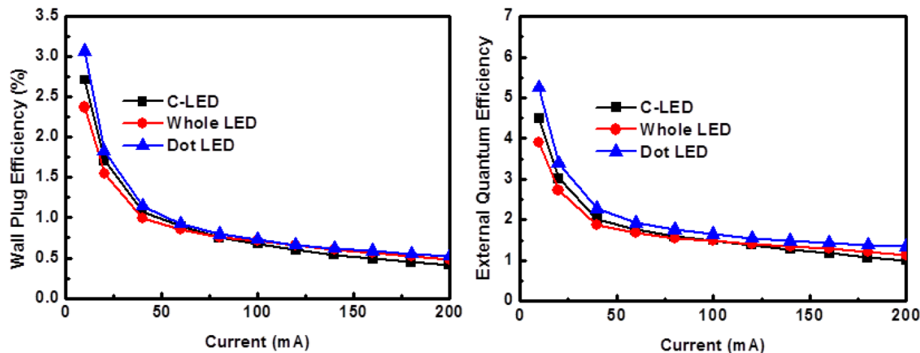

Fig. 7. (a) Wall-plug efficiencies and (b) EQEs of the three types of LEDs as functions of injection current.

Based on the results, the current-spreading path and photon path of the three LEDs were proposed and are schematically illustrated in Figs. 8(a) and 8(b). In Fig. 8(a), common phenomenon current crowded near the electrode edge was exhibited in C-LED. In contrast, in the W-LED structure, the injection current was able to spread in the ZGO thin film, resulting in uniform current spreading and superior electrical properties. To reduce the optical absorption of the ITO film in the DUV region, dot-ITO was employed in the D-LED. The drawback of the D-LED is that the series resistance is increased because of a reduction in the ITO/p-GaN ohmic contact area. These results are consistent with the *I–V* characteristics shown in Fig. 5. Although ITO can create an ohmic contact with p + GaN, the current will flow through the shorter path. Most current flowed through the p-pad and spread by ITO, resulting in a small forward voltage. Nevertheless, it easily occurred the current crowding and shown the output power saturation shown in Fig. 6(a). In the W-LED, the current was injected though the ZGO and then the entire ITO layer. Because the resistivity of ZGO is higher than that of ITO, the current spreading in the W-LED is enhanced compared to in the C-LED, resulting in similar *I–V* characteristics to the C-LED. As the ITO fabricated into dot patterns, it enforces the current spreading more wider than that of W-LED. Nevertheless, only partial

Optics EXPRESS

of ITO plays the low resistivity, causing the D-LED to show worse *I–V* characteristics. Figure 8(b) shows the photon paths for the three types of DUV LEDs. It can be found that the light was absorbed by ITO layer so that active layer emitting light incapable escape form LED inside (C-LED), which results in decreasing LEE. With the introduction of the ZGO + dot-ITO structure, most of the photons could escape from the LED chip, increasing the LEE and the light output power in the D-LED. It is worth mentioning that ZGO can play the light extraction due to the refractive index matching. Not only, the light emitting in the MQW can be escaped from the region without ITO dots. Thus, the D-LED presented the best light output power among the tested devices (Fig. 6).

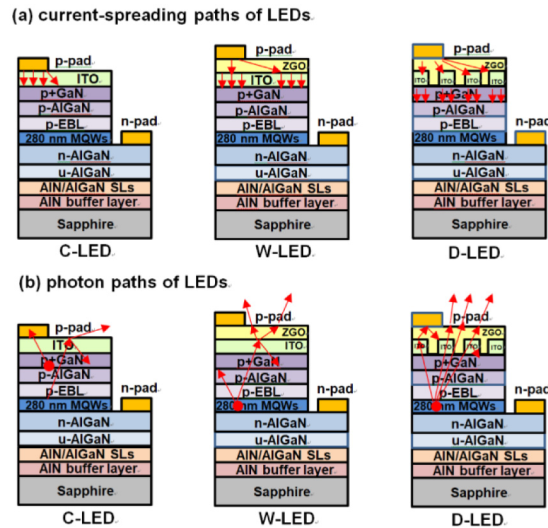

Fig. 8. Schematic diagrams showing the (a) current-spreading paths and (b) photon paths of the three LEDs.

4. Conclusions

The light output, transmittance, and current spreading in DUV AlGaN-based LEDs were improved by incorporating a ZGO TCE layer deposited by MOCVD. At a wavelength of 280 nm, the 200-nm-thick ZGO films showed higher transmittance (93.2%) than the ITO films (28.3%). The output power of the D-LED was enhanced by 32.8% compared to that of the C-LED at an injection current of 200 mA. The results indicate that transparent ZGO films are promising TCEs for p-type electrodes in DUV LED applications.

Funding

Ministry of Science and Technology (MOST) Taiwan (MOST 105-2221-E-009-183-MY3, 104-2221-E-009-199-MY3); Hsinchu Science Park (104A23); ITRI (G101W3402W and G251RA302W).